

***In-materia* speech recognition**

Mohamadreza Zolfagharinejad¹, Julian Büchel², Lorenzo Cassola¹, Sachin Kinge³,
Ghazi Sarwat Syed², Abu Sebastian², Wilfred G. van der Wiel^{1,4†}

¹NanoElectronics Group, MESA+ Institute for Nanotechnology and BRAINS Center for
Brain-Inspired Nano Systems, University of Twente, PO Box 217, Enschede 7500 AE, The
Netherlands.

²IBM Research - Europe, Säumerstrasse 4, 8803 Rüschlikon, Switzerland

³Materials Research and Development, Toyota Motor Europe, B-1930 Zaventem, Belgium

⁴Institute of Physics, University of Münster, 48149 Münster, Germany

†Correspondence to: W.G.vanderWiel@utwente.nl

With the rise of decentralized computing, as in the Internet of Things, autonomous driving, and personalized healthcare, it is increasingly important to process time-dependent signals ‘at the edge’ efficiently: right at the place where the temporal data are collected, avoiding time-consuming, insecure, and costly communication with a centralized computing facility (or ‘cloud’). However, modern-day processors often cannot meet the restrained power and time budgets of edge systems because of intrinsic limitations imposed by their architecture (von Neumann bottleneck) or domain conversions (analogue-to-digital and time-to-frequency). Here, we propose an edge temporal-signal processor based on two *in-materia* computing systems for both feature extraction and classification, reaching a software-level accuracy of $96.2 \pm 0.8\%$ for the TI-46-Word speech-recognition task. First, a nonlinear, room-temperature dopant-network-processing-unit (DNPU)^{1,2} layer realizes analogue, time-domain feature extraction from the raw audio signals, similar to the human cochlea. Second, an analogue in-memory computing (AIMC) chip³, consisting of memristive crossbar arrays, implements a compact neural network trained on the extracted features for classification. With the DNPU feature extraction consuming ~ 100 nW and AIMC-based classification having the potential for less than 10 fJ per multiply-accumulate operation⁴, our findings offer a promising avenue for advancing the compactness, efficiency, and performance of heterogeneous smart edge processors through *in-materia* computing hardware.

Evolution has endowed the human ear with an ingenious sound preprocessing system that performs two domain conversions. Hair cells on the basilar membrane in the cochlea decompose sound waves into their frequency components (time-to-frequency conversion) and convert their mechanical vibrations into electrical signals (mechanical-to-electrical conversion)⁵, which are transmitted to the brain by the auditory nerve for cognitive recognition and interpretation (Fig. 1a)⁶. The auditory system, with its active subsystems, not only converts acoustic waveforms into neural spikes but also *generates* additional tones⁷. As the hair cell vibrations do not increase linearly with the sound intensity and the cochlea exhibits an active feedback mechanism, non-harmonic frequencies (distortions) are generated (Fig. 1a). This *compressive* nonlinearity is crucial for the sensitivity, frequency selectivity, and dynamic range in hearing⁷.

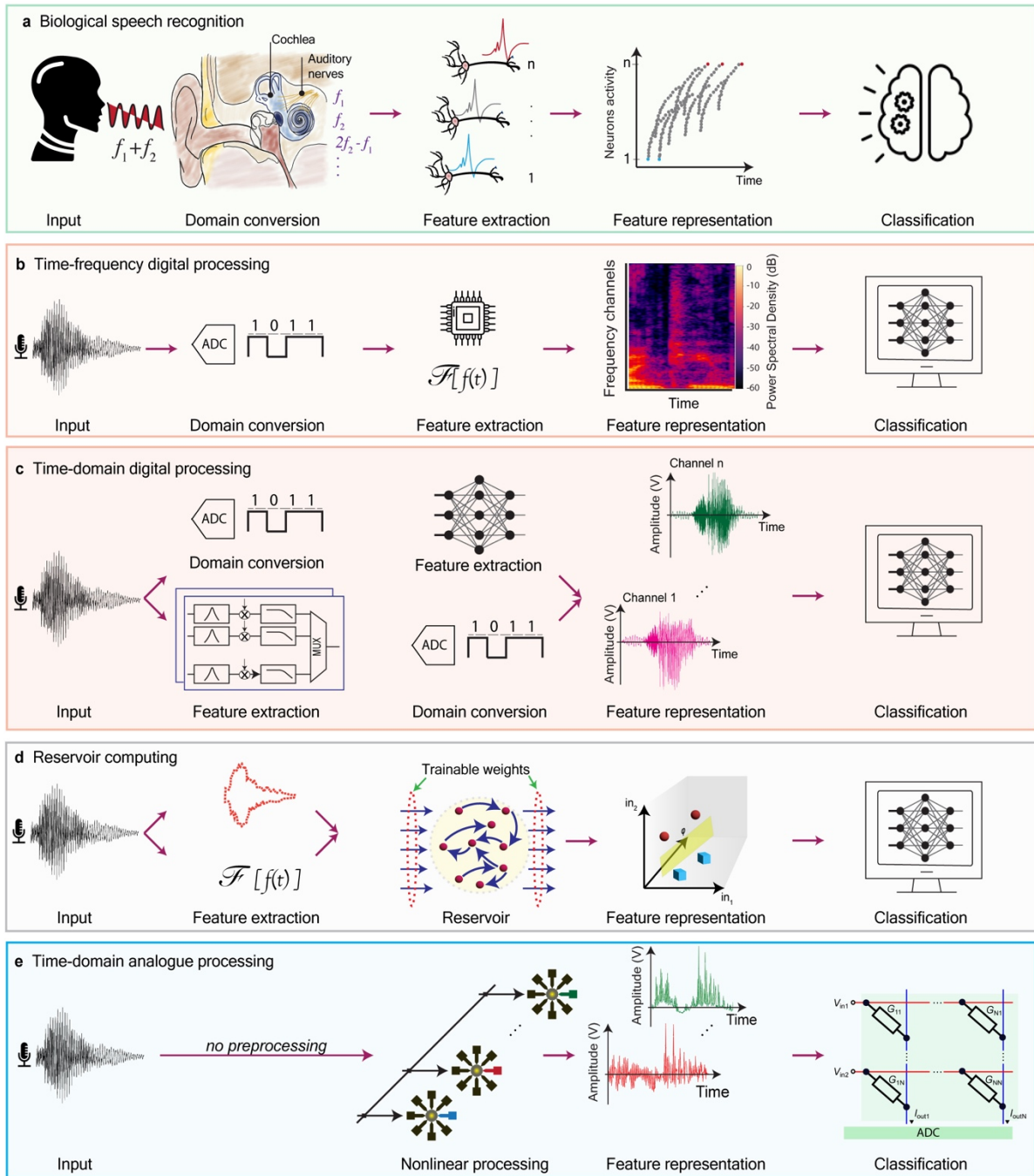


Figure 1. Overview of speech recognition approaches. (a) Biological speech recognition. As an example, when a sound with two frequencies f_1 and f_2 ($f_2 > f_1$), enters the ear, a family of distortion products, such as $2f_1 - f_2$, is generated due to the nonlinear active feedback system in the cochlea^{7,8}. The hair cells on the basilar membrane connected to the auditory nerve endings (1 to n) incorporate two domain conversions to convert the incoming time-dependent acoustic signal into electrical spike-encoded frequency-dependent information (features) to be further processed (classified) by the brain. (b) Time-frequency digital processing method. After analogue-to-digital conversion (ADC), frequency decomposition by a feature-extracting model $F[f(t)]$, such as Lyon's artificial-

cochlea model⁹, is required prior to the classification. **(c)** Time-domain digital processing method. Upper part: in addition to classification, a neural network performs feature extraction by learning (bandpass) filters in the time domain. Lower part: an analogue filter bank extracts frequency features directly from the time-dependent, analogue signal prior to the classification. **(d)** Reservoir computing method. After feature extraction in the time (upper part¹⁰) or frequency domain (lower part), the preprocessed data are projected into a high-dimensional feature space, making the subsequent linear classification simpler. **(e)** Time-domain analogue processing approach (this work). The nonlinear transform provided by dopant network processing units (DNPUs) extracts temporal features and reduces the classification complexity without the need for any additional preprocessing. An analogue in-memory computing (AIMC) chip consisting of a crossbar array of memristive devices is used to efficiently incorporate the classification.

The in-ear preprocessing thus provides real-time, low-power encoding, significantly reducing the data needed to represent raw auditory information.

Computerized audio signal processing, particularly automatic speech recognition (ASR), commonly incorporates three domain conversions (Fig. 1b). First, a microphone converts the acoustic waveform into an analogue electrical signal; second, this signal is digitized using an analogue-to-digital converter (ADC); and third, a short-term Fourier transform (STFT) is applied. The time-to-frequency domain conversion is an important part of the *feature extraction* stage, which – potentially in combination with additional nonlinear data transformations – significantly reduces the complexity of the subsequent classification stage¹¹. The latter can be accomplished by an artificial neural network (ANN), such as a transformer¹², a convolutional neural network (CNN)¹³, a recurrent neural network (RNN)¹⁴, or a combination of those^{15,16}.

ASR models are typically run on specialized hardware, such as application-specific-integrated-circuit accelerators, like a neural engine^{17,18}, graphics processing units¹⁹, or tensor processing units²⁰. The availability of fast and accurate digital hardware has broadened ASR applications, ranging from virtual assistants and customer service systems to transcription services and language-learning platforms. There is particularly an increasing demand for ASR ‘at the edge’ in applications such as always-on e-health medical systems²¹, offline voice assistants¹⁸, and fault-detection systems^{22,23}, where

latency, privacy concerns, or limited connectivity play a role of importance. These requirements demand real-time (or low-latency) and ultra-low-power computing.

However, digital temporal signal processing at the edge is challenging due to expensive domain conversions, complex feature-extraction algorithms²⁴ and the von Neumann bottleneck²⁵. Although combined feature extraction and classification in the time domain (Fig. 1c, upper part) omits the time-to-frequency domain conversion by porting the feature extraction to a neural network^{13,26,27}, it generally requires larger neural networks to extract features from raw data^{28,29}. These difficulties have led to a growing interest in alternative, more efficient approaches³⁰⁻³².

Apart from the conventional (*i.e.*, fully digital) approaches of Figs. 1b and 1c (upper part), emerging ASR can roughly be divided into three categories: artificial-cochlea models in combination with spiking neural networks (SNNs), closest to human hearing (Fig. 1a)¹⁴; analogue filter banks^{33,34} (Fig. 1c, lower part); and reservoir computing (RC, Fig. 1d)^{10,35}. Artificial-cochlea implementations perform feature extraction by converting analogue signals into ‘spike grams’³⁶. Despite the similarity to biology, a spiking hardware classifier realized with, *e.g.*, a digital SNN is required. Lower classification accuracies with spiking features, compared to time-, or frequency-domain features, suggest that the classification step is more difficult³⁷. Although analogue filter banks (Fig. 1c, lower part) do not require digitization for feature extraction, recent demonstrations still require digital classifiers³³. In RC³⁸⁻⁴⁰, the reservoir first projects the temporal input into a higher-dimensional feature space, enabled by its recurrent (multi-timescale) time dynamics, followed by a linear classification layer. However, high classification accuracy requires a complex classification step when the reservoir is fed with time-domain input¹⁰, *e.g.*, a deep CNN²⁹. Alternatively, expensive preprocessing, such as using the mel-frequency cepstral coefficients, is needed when feeding the reservoir with frequency-domain features^{11,24,35,41-44}. Despite promising classification results obtained on the TI-46-Word spoken digit task⁴⁵, edge conditions demand hardware that is not only accurate but also compact and efficient. This requires an approach that simultaneously addresses domain conversions, efficient feature extraction and the von Neumann bottleneck.

In this Article, we present an ASR architecture based on two emerging *in-materia* computing paradigms. First, analogue, time-domain feature extraction is achieved through a circuit that

incorporates one or more dopant network processing units (DNPUs)¹ working at room temperature. Serving as the core of a low-power analogue circuit, the DNPU uniquely establishes biologically plausible feature extraction through a recurrent nonlinear transformation with adjustable frequency selectivity and tuneable characteristic time scales in the millisecond range. Second, for the classification based on the extracted features, we implement a CNN on an analogue in-memory computing (AIMC)³ chip. Crossbar arrays of synaptic phase-change-memory (PCM) unit cells perform the matrix-vector multiplication operations for the CNN, mitigating the von Neumann bottleneck. We assess the performance of these combined *in-materia* approaches using the TI-46-Word spoken digits dataset, achieving a near-software-equivalent accuracy of $96.2 \pm 0.8\%$.

Time-domain processing with DNPUs

DNPUs possess the three characteristics crucial for biologically plausible time-domain speech recognition: frequency selectivity, tuneable nonlinearity, and sensory memory within the desired millisecond range in audio recognition. Figure 2(a) shows a false-colour atomic-force-microscopy (AFM) image of a DNPU and the measurement circuitry. The active region of the DNPU consists of a disordered network of hopping sites in silicon, surrounded by eight electrodes (one input, one output, six controls). This network features a complex energy landscape and highly nonlinear charge transport tuneable via the control voltages to achieve specific functionalities, such as Boolean logic, nonlinear classification, and feature extraction^{1,2,46} (see Methods for fabrication details).

In our earlier work on static (time-independent) tasks^{1,2,46}, we operated the DNPUs at 77 K with voltage input and current output, using a transimpedance amplifier (Extended Data Fig. 1), effectively shorting the stray capacitance of the readout circuit, and minimizing the response time. Here, for the first time, we operate at room temperature (see Methods) and measure the output as a *voltage*. Specifically, we use a buffer circuit with a large input impedance ($> 1 \text{ G}\Omega$) at the DNPU output, so that the external capacitance C_{ext} ($\sim 10\text{-}100 \text{ pF}$) can no longer be neglected (Fig. 2a). Together with the intrinsic nonlinear DNPU resistance and capacitance, these features now give rise to a highly nontrivial transformation with a tuneable characteristic timescale in the $\sim\text{ms}$ timescale. In the inset of Fig., 2b we show the distribution of these timescales, corresponding to 500 sets of random control voltages.

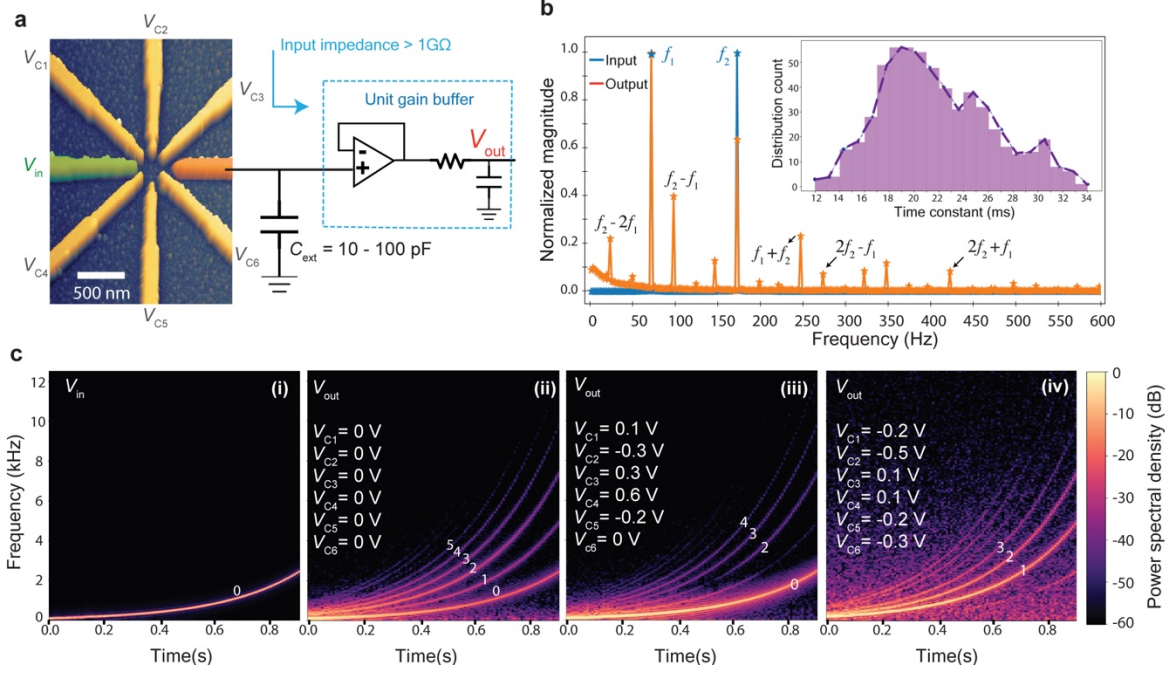


Figure 2. Tuneable nonlinearity and short-term memory characterization in a DNPU at room temperature. **a**, Atomic-force-microscopy image of an 8-electrode DNPU and schematic measurement circuit with external capacitance C_{ex} (~ 10 - 100 pF) and a >1 G Ω input impedance buffer. **b**, Fourier transform of a two-tone input signal (blue, f_1 and f_2) and the DNPU response (orange), showing (sub-)harmonics and distortions. Similar to the frequency response of a human cochlea, the output signal contains a family of distortion products ($|(n+1)f_1 - nf_2|$) of progressively higher frequencies and lower magnitudes⁷. Inset: Histogram of time constants (τ is the time for the output to reach 63% of V_{max}) of V_{out} as a response to a 1 V step input with a rising time <20 μ s for 500 randomly configured control-voltage sets. **c(i)**, Power spectral density (PSD) of chirp input voltage signal $V_{in}(t) = A \sin \left[2\pi f_0 \left(\frac{k^t - 1}{\ln(k)} \right) + \varphi_0 \right]$, where A is the amplitude, f_0 the starting frequency, k the rate of exponential change in frequency, φ_0 the initial phase at $t = 0$, f_1 the final frequency, and T the duration of the signal. As shown in Fig. 2c(i), these values are set to $A = 0.75$ V, $\varphi_0 = -\frac{\pi}{2}$, $k = \left(\frac{f_1}{f_0} \right)^{\frac{1}{T}}$, $T = 1$ s, $f_1 = 2$ kHz, and $f_0 = 100$ Hz. **c(ii)**, PSD of output voltage $V_{out}(t)$ in response to the input signal of c(i) with zero volts on all controls, showing up to 5 harmonics. **c(iii)**, Idem for a set of random control voltages. **c(iv)**, Idem, for a different set of random control voltages.

Figure 2b shows the response of the DNPU circuit to a two-tone input, where a signal with two frequencies ($f_1 = 74$ Hz, $f_2 = 174$ Hz) is fed to the DNPU input (blue). The Fourier transform of the output signal is shown in orange, where, by changing the control voltages, the magnitude of these

distortion products can be adjusted. Figures 2c(ii)-(iv) show the output spectrograms for three different sets of control voltages in response to an exponential chirp input signal (Fig. 2c(i)). In Fig. 2c(ii), all control electrodes are set to 0 V with respect to the ground. The output voltage contains up to the 5th harmonic of the input signal, indicating the presence of strong nonlinearities. Importantly, these harmonics can be tuned by the control voltages, as shown in Figs. 2c(iii) and 2c(iv). For example, harmonics can be selectively created or removed, including the fundamental tone.

The DNPU output voltage is determined by the complex potential landscape of the active region, which in turn depends on the potential at each electrode. Similar to a state-dependent system, when the charge stored at the output capacitor changes, the potential at the output electrode correspondingly alters, modifying the circuit characteristics (*i.e.*, τ), effectively forming an active-feedback system, which introduces recurrency and short-term memory (Fig. 3a). In concrete, the charge on C_{ex} at time $t = t_0$ influences the DNPU behaviour at $t = t_0 + \Delta t$, given $\Delta t \lesssim R_{\text{DNPU}}(t_0) C_{\text{ex}}$, where $R_{\text{DNPU}}(t_0)$ is the DNPU resistance measured at $t = t_0$ between the input and output electrodes with applying the control voltages $V_{C1}, V_{C2}, \dots, V_{C6}$. Supplementary Info. Note 1 provides details for measurements and experimental results indicating the recurrent form of fading memory based on the variable impedance of the DNPU.

Frequency selectivity and short-term (fading) memory are key characteristics of neural network models for temporal data processing^{10,13}. For example, CNN models use large kernel sizes for the first convolution layer, typically a ~ 10 ms receptive field, to capture temporal features from raw audio^{27,28}. The first layer extracts low-level features, while the deeper layers with smaller kernel sizes construct higher-level features and perform classification²⁷. Interestingly, the overall accuracy of an end-to-end CNN classifier is only slightly affected by training the initial layer and remains acceptable even with random initializations¹³. Leaving the first layer untrained, *i.e.*, feature extraction with random software filter banks⁴⁷ can reduce the training costs⁴⁸. In the inference phase, however, the first layer is the most computationally expensive part of the network as the large kernel size demands many multiply-accumulate (MAC) operations. For example, in a 5-layer CNN for raw audio classification, for inference of a single input sample, the first layer accounts for $\sim 75\%$ of all MAC operations²⁸ (Suppl. Info. Note 2).

TI-46-Word spoken digit task with DNPU feature extraction and a software classifier

Motivated by insights from biology and conventional speech-recognition systems, we propose a DNPU circuit with its *in-situ* adjustable nonlinearity (Figs. 2b and 2c) and tuneable time dynamics (Fig. 2b, inset) to implement an *in-materia* time-domain feature extractor and combine it first with a software classifier model (we discuss an *in-materia* classifier below). To evaluate the performance of this hybrid

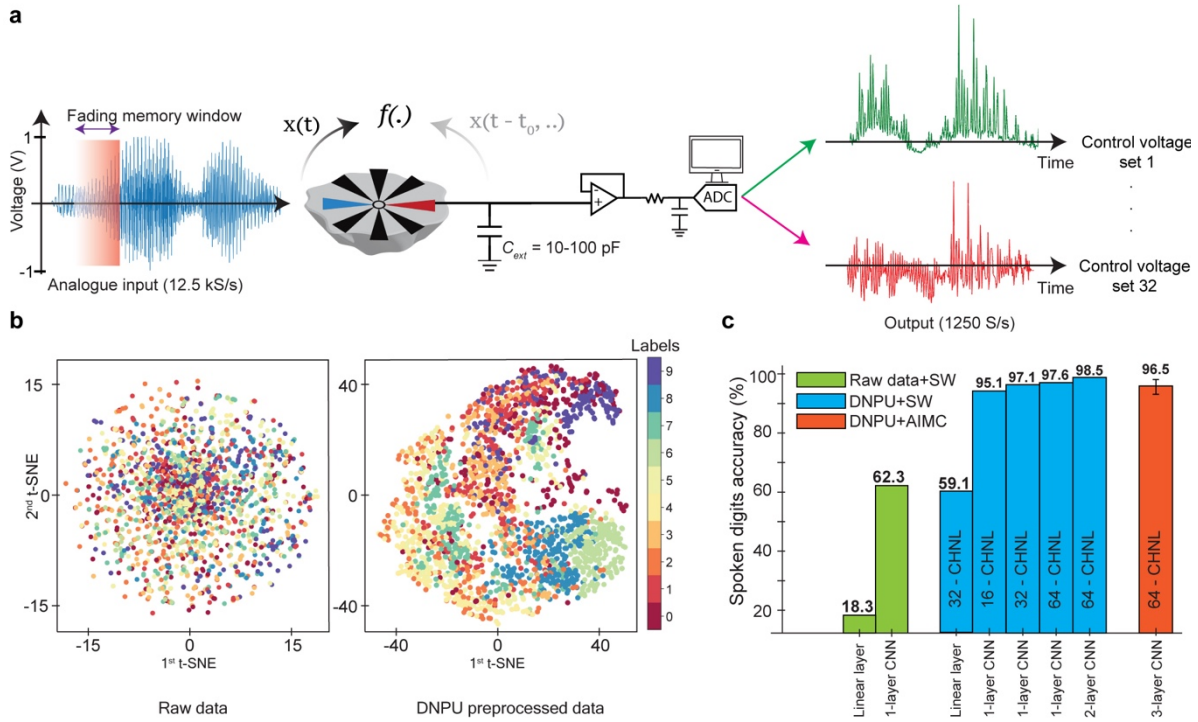


Figure 3. DNPU analogue feature extraction for speech recognition. **a**, Schematic of DNPU (nonlinear function noted as $f(\cdot)$) fed with analogue time-dependent input $x(t)$ (blue electrode), voltage measured at the orange electrode and constant control voltages (black electrodes). Every set of control voltages results in a unique transformed signal (green and red curves shown as examples) and forms an output channel with $10\times$ lower sample rate compared to the raw input signal (see Methods). **b**, t-distributed stochastic neighbour encoding (t-SNE) visualization for the female subset of the TI-46-Word spoken digit dataset before and after preprocessing by a single, untrained DNPU (one configuration out of 32 sets of randomly chosen control voltages). The output data show that the DNPU preprocessing helps clustering utterances of the same digit, simplifying later classification. **c**, Comparison of the classification accuracy for linear and CNN classifier models without (green) and with (blue and red) DNPU preprocessing for 16, 32, and 64 DNPU channels. The all-hardware (DNPU with the AIMC classifier) result (red) is presented as the mean \pm one standard deviation over ten inference measurements.

system, we use the TI-46-Word spoken digits female subset with 2,075 samples (see Methods). The dataset contains clean utterances from 8 female speakers, divided into train and test subsets. As a trade-off between power consumption and classification accuracy, the dataset is processed 32 times by a single DNPU circuit (Fig. 3a), each time with a different set of random control voltages (in a device-dependent voltage range, see Methods). We refer to each DNPU pass as a channel, thus obtaining 32 channels. Alternatively, one could obtain 32 channels by using 32 different, randomly initialized DNPU in parallel. Also, instead of randomly initialized DNPU, one could use DNPU with control voltages *trained* in an end-to-end fashion together with the software classifier, using backpropagation (see Suppl. Info. Note 3).

The results of the DNPU preprocessing (illustrated by the green and red traces in Fig. 3a) contain fingerprints (or low-level features) of the input data. Similar to contrastive learning⁴⁹, the DNPU preprocessing puts same-labeled instances of the dataset closer together in *time-domain* representation space while keeping dissimilar instances apart. To visualize this, we use t-distributed stochastic neighbour encoding (t-SNE)¹¹, which is a statistical method for visualizing high-dimensional data⁵⁰ (we also used universal manifold approximation and projection (UMAP)⁵¹, see Suppl. Info. Note 4). Figure 3b shows the t-SNE visualization of the original (raw) audio dataset and the same dataset after being processed by a single, untrained DNPU circuit. Compared to the original dataset, well-defined clusters for some digits, such as ‘six’, ‘eight’, and ‘nine’, are observed. However, for other digits, a more scattered distribution is found.

To study the impact of DNPU preprocessing on the overall classification performance, we examined several simple classifier models, with and without DNPU preprocessing (see Methods). As shown in Fig. 3c, a single-layer linear model performs poorly on the raw data (green, ~18%). An additional single convolutional layer with 32 output channels after, or 32-channel DNPU preprocessing (blue) before the linear model improves the overall classification accuracy to ~60%. It is worth noting that the backpropagation-trained software CNN outperforms preprocessing by *randomly* initialized DNPU by only 3% point. If we combine 16-channel DNPU preprocessing with a 1-layer CNN, we achieve 95.1% accuracy (blue), with only ~4,000 learnable parameters. For comparison, recent studies on a subset of the TI-46-Word spoken digits dataset with 500 samples, using the same number of learnable parameters

(4,096), have reported classification accuracies of 78% without¹⁰ and 97% with⁵² frequency-domain feature extraction. Higher accuracies are achieved with 32 or 64 channels and using a 2- or 3-layer CNN software model. With 64-channel DNPU-processed data and a 2- (and also 3-) layer CNN, we now obtain 98.5% overall accuracy (blue), which is comparable to the best-known all-software solutions, such as long short-term memory (LSTM) models⁵².

Frequency selectivity, compressive nonlinearity, and a recurrent form of feedback from the output are key properties of the DNPU circuit that facilitate temporal data processing. These characteristics are indispensable elements for acoustic feature extraction, which are also fundamental in the biological cochlea. To substantiate their importance, in Suppl. Info. Notes 5-7, we compare different filter banks of low- and bandpass filters when they incorporate one or more of the mentioned characteristics. There, we show that having, for instance, a *hyperbolic tangent* compressive nonlinearity can notably improve the feature extraction performance in filter banks. Furthermore, in Suppl. Info. Note 8, we use 64 different *reservoir* models for the feature extraction step, where we can see that although high-level projections of reservoirs are, to some extent, capable of acoustic feature extraction, they perform poorly compared to other methods. Supplementary Table I summarizes the inference accuracy among different preprocessing methods for the same classifier model, indicating the good performance of DNPUs.

Mapping the classifier model on an AIMC chip

As discussed above, DNPU preprocessing effectively extracts time-domain acoustic features that significantly simplify the classification task. However, the classifier model still consumes typically ~40% of the total power consumption in an ASR system³³. In traditional DNN implementations, the energy consumption is dominated by memory access and data transfer between the processor and memory units⁵³. We leverage analogue in-memory computing or AIMC, another *in-materia* computing paradigm, to address this challenge. Memristive materials provide processing *in* non-volatile memories to store the weights of the neural network^{31,54,55}. Below, we discuss the results of a classifier model trained with the features from the DNPU implemented on the IBM HERMES project AIMC chip³ (through a digital interface as the DNPU and AIMC chips are currently physically separated).

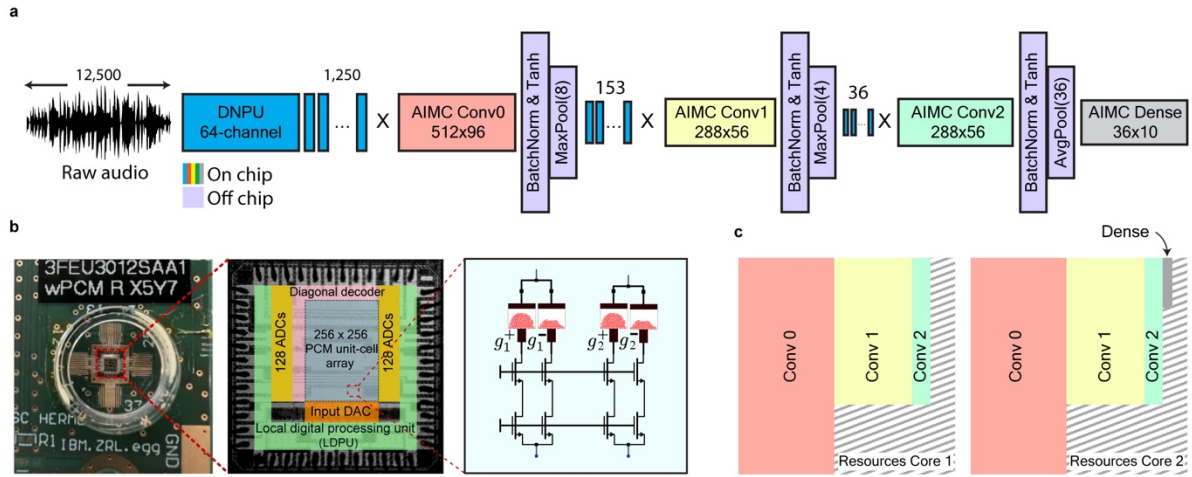


Figure 4. Schematic of a hybrid convolutional neural network (CNN) architecture for *in-materia* speech recognition. **a**, CNN architecture. A 64-channel DNPU convolution converts audio signals into 64-D input to the AIMC with a down-sampling rate of 10 (Details in Extended Data Figure 3). The first AIMC convolution layer has a kernel size of 8, and the rest of 3. Batch normalization, activation functions, and pooling operations are performed off-chip. **b**, A photograph of the IBM HERMES project chip and the architecture of the chip containing 256×256 synaptic unit cells, each comprising of 4 phase-change-memory (PCM) devices organized in a differential configuration, ADC/DAC arrays, and on-chip local digital processing units (LDPU). **c**, Schematic representation of resource utilization for the 3-layer CNN classifier model implemented on two tiles of the AIMC chip.

We implemented a best-performing model with three convolutional layers on the HERMES project chip trained with the data from 64 DNPU measurement channels (Fig. 4a, see Methods for other configurations). The CNN training includes a standard and a retraining phase to enhance the network model's resilience to analogue noise⁵⁶. We used the open-source IBM analogue hardware acceleration kit⁵⁷ to add weight and activation noise, perform weight clipping, and incorporate ADC quantization noise during the retraining phase (see Methods for more details). The learned network weights are then transferred to each synaptic PCM unit cell as analogue conductance values using gradient-descent-based programming (GDP)⁵⁸. The CNN training includes a standard and a retraining phase to enhance the network model's resilience to analogue noise⁵⁶. We used the open-source IBM analogue hardware acceleration kit⁵⁷ to add weight and activation noise, perform weight clipping, and incorporate ADC quantization noise during the retraining phase (see Methods for more details). The learned network

weights are then transferred to each synaptic PCM unit-cell as analogue conductance values using gradient-descent-based programming (GDP)⁵⁸. The two combined *in-materia* systems achieve a near-software inference accuracy ($96.2 \pm 0.8\%$ averaged over 10 repetitions, compared to 98.5% for the DNPU with a software classifier) while performing approximately 95% of total operations on novel material systems and offloading less than 5% to digital processors.

Discussion

To the best of our knowledge, this is the first demonstration of bio-plausible, time-domain speech recognition using two *in-materia* computing hardware systems for both feature extraction and classification. The 96.2% end-to-end, all-hardware accuracy (*i.e.*, DNPU preprocessing + AIMC CNN) obtained for the TI-46-Word task in this study is comparable to state-of-the-art software models that have $10\times$ more learnable parameters⁵², and only $\sim 2\%$ point lower than when the classifier is implemented in software (*i.e.*, DNPU + software CNN). We expect that optimizing the AIMC retraining phase, specifically for temporal data processing, can further improve these results. Furthermore, in contrast to the state of the art, our approach achieves high classification rates without the necessity for costly digital feature extraction⁴¹ or a complex classifier model²⁹.

The real-time, analogue DNPU feature extraction not only avoids time- and energy-consuming domain conversions but also significantly simplifies the classification task. We estimate the static power consumption of the single-DNPU circuit of Fig. 2a to be less than 5 nW. The AIMC-based classification has the potential for less than 10 fJ per multiply-accumulate operation⁴.

As every DNPU is unique, DNPU-based feature extraction will always require the subsequent classifier to be trained accordingly. For real-life applications, it will be practical if this training is performed online in an adaptive fashion. While the inability to copy the parameters from one system to another is a disadvantage, it could be an asset for applications where safety and privacy are critical. Presently, the DNPU and AIMC layers are still physically separated. However, backend-of-the-line and heterogeneous integration⁵⁹ should allow for integration of DNPUs and AIMC on the same chip. Also, a single physical DNPU has been time-multiplexed in this work. To fully exploit our platform's potential, we need to scale up DNPU circuits in mainstream CMOS technology and use parallel multi-

channel feature extraction. Although we have benchmarked our method for a speech-recognition task, we expect it to be generally applicable to temporal signal processing at the edge, such as video or EEG/ECG data classification. Our results demonstrate that combining two *in-materia* computing hardware platforms for feature extraction and classification can simultaneously address efficiency, accuracy, and compactness, providing sustainable edge computing solutions.

Online content

Any methods, additional references, Nature Research reporting summaries, source data, extended data, supplementary information, acknowledgements, peer review information; details of author contributions and competing interests; and statements of data and code availability are available at <https://doi.org/xxx>.

References

- 1 Chen, T. et al. Classification with a disordered dopant-atom network in silicon. *Nature* **577**, 341-345 (2020).
- 2 Ruiz Euler, H.-C. et al. A deep-learning approach to realizing functionality in nanoelectronic devices. *Nat. Nanotechnol.* **15**, 992-998 (2020).
- 3 Le Gallo, M. et al. A 64-core mixed-signal in-memory compute chip based on phase-change memory for deep neural network inference. *Nat. Electron.* **6**, 1-14 (2023).
- 4 Jain, S. et al. A heterogeneous and programmable compute-in-memory accelerator architecture for analog-AI using dense 2-D mesh. *IEEE Trans. Very Large Scale Integration (VLSI) Systems* **31**, 114-127 (2022).
- 5 Carney, L. H. A model for the responses of low-frequency auditory-nerve fibers in cat. *J. Acoust. Soc. Am.* **93**, 401-417 (1993).
- 6 Smotherman, M. S. & Narins, P. M. Hair cells, hearing and hopping: a field guide to hair cell physiology in the frog. *J. Exp. Biol.* **203**, 2237-2246 (2000).

- 7 Hudspeth, A. J. Integrating the active process of hair cells with cochlear function. *Nat. Rev. Neurosci.* **15**, 600-614 (2014).
- 8 Ren, T., He, W., Scott, M. & Nuttall, A. L. Group delay of acoustic emissions in the ear. *J. Neurophysio.* **96**, 2785-2791 (2006).
- 9 Lyon, R. A computational model of filtering, detection, and compression in the cochlea. In *Proc. 1982 IEEE International Conference on Acoustics, Speech, and Signal Processing* 1282-1285 (IEEE, 1982).
- 10 Dion, G., Mejaouri, S. & Sylvestre, J. Reservoir computing with a single delay-coupled non-linear mechanical oscillator. *J. Appl. Phys.* **124**, 152132 (2018).
- 11 Abreu Araujo, F. et al. Role of non-linear data processing on speech recognition task in the framework of reservoir computing. *Sci. Rep.* **10**, 1-11 (2020).
- 12 Dong, L., Xu, S. & Xu, B. Speech-transformer: a no-recurrence sequence-to-sequence model for speech recognition. In *Proc. 2018 IEEE International Conference on Acoustics, Speech and Signal Processing*. 5884-5888 (IEEE, 2018).
- 13 Abdoli, S., Cardinal, P., & Koerich, A. L. End-to-end environmental sound classification using a 1D convolutional neural network. *Expert Syst. Appl.* **136**, 252-263 (2019).
- 14 Gao, C., Neil, D., Ceolini, E., Liu, S.-C. & Delbruck, T. DeltaRNN: A Power-efficient recurrent neural network accelerator. In *Proc. 2018 ACM/SIGDA International Symposium on Field-Programmable Gate Arrays*. 21-30 (ACM, 2018).
- 15 Hsu, W.-N., Zhang, Y., Lee, A. & Glass, J. Exploiting Depth and Highway Connections in Convolutional Recurrent Deep Neural Networks for Speech Recognition. In *2016 Proc. International Conference on Spoken Language Processing*. 395-399 (2016).
- 16 Gulati, A. et al. Conformer: Convolution-augmented transformer for speech recognition. Preprint at: <https://arXiv.org/abs/2005.08100> (2020).

- 17 Izbassarova, A., Duisembay, A. & James, A. P. *Speech Recognition Application Using Deep Learning Neural Network*. In *Deep Learning Classifiers with Memristive Networks: Theory and Applications*, (ed. James, A.) 69-79 (Springer, Cham. 2020).
- 18 Isyanto, H., Arifin, A. S. & Suryanegara, M. Performance of smart personal assistant applications based on speech recognition technology using IoT-based voice commands. In *2020 International conference on information and communication technology convergence*. 640-645 (IEEE, 2020).
- 19 Kim, C. et al. A review of on-device fully neural end-to-end automatic speech recognition algorithms. In *2019 IEEE Automatic Speech Recognition and Understanding Workshop (ASRU)*. 562-569 (IEEE, 2019).
- 20 Gondi, S. & Pratap, V. Performance evaluation of offline speech recognition on edge devices. *Electronics* **10**, 2697 (2021).
- 21 Raza, A. et al. Heartbeat sound signal classification using deep learning. *Sensors* **19**, 4819 (2019).
- 22 Tran, T., Pham, N. T. & Lundgren, J. A deep learning approach for detecting drill bit failures from a small sound dataset. *Sci. Rep.* **12**, 9623 (2022).
- 23 Wu, Z., Wan, Z., Ge, D. & Pan, L. Car engine sounds recognition based on deformable feature map residual network. *Sci. Rep.* **12**, 1-13 (2022).
- 24 Luo, Y. & Mesgarani, N. Conv-tasnet: Surpassing ideal time–frequency magnitude masking for speech separation. *IEEE/ACM Trans. Audio Speech Lang. Process.* **27**, 1256-1266 (IEEE, 2019).
- 25 Sebastian, A., Le Gallo, M., Khaddam-Aljameh, R. & Eleftheriou, E. Memory devices and applications for in-memory computing. *Nat. Nanotechnol.* **15**, 529-544 (2020).

- 26 Hoshen, Y., Weiss, R. J. & Wilson, K. W. Speech acoustic modeling from raw multichannel waveforms. In Proc. *2015 IEEE international conference on acoustics, speech and signal processing*. 4624-4628 (IEEE, 2015).
- 27 Sainath, T., Weiss, R. J., Wilson, K., Senior, A. W. & Vinyals, O. Learning the speech front-end with raw waveform CLDNNs. In 2016 Proc. *International Conference on Spoken Language Processing* (2015).
- 28 Dai, W., Dai, C., Qu, S., Li, J. & Das, S. Very deep convolutional neural networks for raw waveforms. In Proc. *2017 IEEE international conference on acoustics, speech and signal processing*. 421-425 (IEEE, 2017).
- 29 Shougat, M. R. E. U., Li, X., Shao, S., McGarvey, K. & Perkins, E. Hopf physical reservoir computer for reconfigurable sound recognition. *Sci. Rep.* **13**, 8719 (2023).
- 30 Jaeger, H., Noheda, B. & Van Der Wiel, W. G. Toward a formal theory for computing machines made out of whatever physics offers. *Nat. Commun.* **14**, 4911 (2023).
- 31 Zolfagharinejad, M., Alegre-Ibarra, U., Chen, T., Kinge, S. & van der Wiel, W. G. Brain-inspired computing systems: a systematic literature review. *The European Physical Journal B* **97**, 70 (2024).
- 32 Tye, N. J., Hofmann, S. & Stanley-Marbell, P. Materials and devices as solutions to computational problems in machine learning. *Nat. Electron.* **6**, 479-490 (2023).
- 33 Villamizar, D. A., Muratore, D. G., Wieser, J. B. & Murmann, B. An 800 nw switched-capacitor feature extraction filterbank for sound classification. *IEEE Trans. Circuits Syst. I: Regular Papers* **68**, 1578-1588 (2021).
- 34 Li, Y. et al. Memristive Field-Programmable Analog Arrays for Analog Computing. *Adv. Mater.* **35**, 2206648 (2023).
- 35 Romera, M. et al. Vowel recognition with four coupled spin-torque nano-oscillators. *Nature* **563**, 230-234 (2018).

- 36 Liu, S.-C., van Schaik, A., Minch, B. A. & Delbruck, T. Asynchronous Binaural Spatial Audition Sensor With $2 \times 64 \times 4$ Channel Output. *IEEE Trans. Biomed. Circuits Sys.* **8**, 453-464 (2013).
- 37 Gao, C. et al. Real-time speech recognition for IoT purpose using a delta recurrent neural network accelerator. In Proc. 2019 *IEEE International Symposium on Circuits and Systems*. 1-5 (IEEE, 2019).
- 38 Lukoševičius, M. & Jaeger, H. Reservoir computing approaches to recurrent neural network training. *Comput. Sci. Rev.* **3**, 127-149 (2009).
- 39 Maass, W., Natschläger, T. & Markram, H. Real-time computing without stable states: A new framework for neural computation based on perturbations. *Neural Comput.* **14**, 2531-2560 (2002).
- 40 Liang, X. et al. Physical reservoir computing with emerging electronics. *Nat. Electron.* **7**, 193-206 (2024).
- 41 Msiska, R., Love, J., Mulkers, J., Leliaert, J. & Everschor-Sitte, K. Audio classification with skyrmion reservoirs. *Adv. Intel. Sys.* **5**, 2200388 (2023).
- 42 Usami, Y. et al. In-materio reservoir computing in a sulfonated polyaniline network. *Adv. Mater.* **33**, 2102688 (2021).
- 43 Cai, H. et al. Brain organoid reservoir computing for artificial intelligence. *Nat. Electron.* **6**, 1032-1039 (2023).
- 44 Torrejon, J. et al. Neuromorphic computing with nanoscale spintronic oscillators. *Nature* **547**, 428-431 (2017).
- 45 Appeltant, L. et al. Information processing using a single dynamical node as complex system. *Nat. Commun.* **2**, 468 (2011).

- 46 Ruiz-Euler, H.-C. et al. Dopant network processing units: towards efficient neural network emulators with high-capacity nanoelectronic nodes. *Neuromorph. Comput. Engin.* **1**, 024002 (2021).
- 47 Keshavarzian, A., Salehinejad, H. & Valaee, S. Representation learning of clinical multivariate time series with random filter banks. In Proc. *2023 IEEE International Conference on Acoustics, Speech and Signal Processing*. 1-5 (IEEE, 2023).
- 48 Pons, J. & Serra, X. Randomly weighted CNNs for (music) audio classification. In Proc. *2019 IEEE international conference on acoustics, speech and signal processing*. 336-340 (IEEE, 2019).
- 49 Khosla, P. et al. Supervised contrastive learning. *Adv. Neural inf. Process. Syst.* **33**, 18661-18673 (2020).
- 50 Van der Maaten, L. & Hinton, G. Visualizing data using t-SNE. *J. Mach. Learn. Res.* **9** (2008).
- 51 McInnes, L., Healy, J. & Melville, J. Umap: Uniform manifold approximation and projection for dimension reduction. Preprint at <https://arxiv.org/abs/1802.03426> (2018).
- 52 Moon, J. et al. Temporal data classification and forecasting using a memristor-based reservoir computing system. *Nat. Electron.* **2**, 480-487 (2019).
- 53 Ambrogio, S. et al. An analog-AI chip for energy-efficient speech recognition and transcription. *Nature* **620**, 768-775 (2023).
- 54 Rao, M. et al. Thousands of conductance levels in memristors integrated on CMOS. *Nature* **615**, 823-829 (2023).
- 55 Yao, P. et al. Fully hardware-implemented memristor convolutional neural network. *Nature* **577**, 641-646 (2020).

- 56 Rasch, M. J. et al. Hardware-aware training for large-scale and diverse deep learning inference workloads using in-memory computing-based accelerators. *Nat. Commun.* **14**, 5282 (2023).
- 57 Le Gallo, M. et al. Using the IBM Analog In-Memory Hardware Acceleration Kit for Neural Network Training and Inference. *APL Mach. Learn.* **1** (4) (2023).
- 58 Büchel, J. et al. in *2022 International Electron Devices Meeting (IEDM)*. **33**(1) (IEEE, 2022).
- 59 Chen, M.-F., Chen, F.-C., Chiou, W.-C. & Doug, C. System on Integrated Chips (SoIC(TM) for 3D Heterogeneous Integration. In Proc. 2019 *IEEE 69th Electronic Components and Technology Conference (ECTC)*. 594-599 (IEEE, 2019).

Methods

DNPU fabrication and room-temperature operation

A lightly n-doped silicon wafer (resistivity $\rho \sim 5 \Omega \cdot \text{cm}$) is cleaned and heated for 4 hours in a furnace at 1100 °C for dry oxidation, producing a 280 nm thick SiO₂ layer. Photolithography and chemical etching are used to selectively remove the silicon oxide in $26 \times 60 \mu\text{m}$ windows. A second, 35 nm SiO₂ layer is needed for the desired dopant concentration. Ion implantation of B⁺ ions is performed at 9 keV with a dose of $3.5 \cdot 10^{14} \text{ cm}^{-2}$. After implantation, rapid thermal annealing (1050 °C for 7 s) is carried out to activate the dopants. The second oxide layer is removed by buffered hydrofluoric acid (1:7; 45 seconds) and then the wafer is diced into $1 \times 1 \text{ cm}$ pieces. E-beam lithography and e-beam evaporation are used, respectively, for creating the (1.5 nm Ti/25 nm Pd) electrodes. Finally, reactive ion etching (CHF₃ and O₂, (25:5)) is used to etch (30-40 nm) the silicon until the desired dopant concentration is obtained.

We have consistently realized room-temperature functionality, characterized by an observed activation energy of $\sim 0.4 \text{ eV}$. This energy scale, which cannot be associated with the (much smaller) B ionization energy, indicates a trap-assisted transport mechanism, where a high concentration of impurities prevents normal band conduction. P_b centers (dangling bonds at the Si-SiO₂ interface) seem to be the most likely candidates for this role, owing to their position in the silicon band gap⁶⁰, which matches with the measured activation energy, and the fact that they are ambipolar (the same results were obtained for As-doped samples) and electronically active. A detailed study of the charge transport mechanism and the interplay of the intentional and unintentional dopants at room temperature will be presented elsewhere.

DNPU measurement circuitry

We use a National Instruments (NI) C-series voltage output module (NI-9264) to apply input and control voltages to the DNPU. The NI-9264 is a 16-bit digital-to-analogue converter (DAC) with a slew rate of 4 V/ μs and a settling time of 15 μs for a 100 pF capacitive load and 1 V step. As shown in Fig. 2a, a small parasitic capacitance ($\sim 10\text{-}100 \text{ pF}$) to ground is present at the DNPU output. In contrast to our previous work^{1,2}, we do not measure the DNPU output current but the output voltage without

amplification. In Refs. [1,2,46], the device output was virtually grounded by the operational amplifier used for current-to-voltage conversion (Extended Data Fig. 1). Thus, the external capacitance was essentially short-circuited to ground, and no time dynamics was observed. In the present study, we directly measure and digitize the DNPU output voltage with the NI C-series voltage input module (NI-9223; input impedance $>1 \text{ G}\Omega$). A large input impedance, *i.e.*, more than ten times the DNPU resistance, is necessary to ensure that the time dynamics of the DNPU circuit is measurable.

DNPU optimization

The DNPU control electrodes are used to tune the functionality for both linear and nonlinear operation regimes. Applying control voltages $\geq 500 \text{ mV}$ pushes the DNPU into its linear regime. Furthermore, higher control voltages make the device more conductive, leading to a faster discharge of the external capacitor and, thus, a smaller time constant. In this work, we choose control voltages randomly between -0.4 V and 0.4 V except for the end-to-end training of neural networks with DNPUs in the loop (see Suppl. Info. Note 1). For electrodes directly next to the output, we reduce this range by a factor of two because these control voltages have a stronger influence on the output voltage.

DNPU static power measurement

To estimate the DNPU energy efficiency, we measured the static power consumption, P_{static} , for ten different sets of random control voltages and averaged the results. In every configuration, a constant DC voltage is applied to each electrode, and the resulting current through every electrode is measured sequentially using a Keithley 236 source measure unit (SMU). P_{static} is calculated according to

$$P_{\text{static}} = \sum_{k=0}^{N-1} V_k I_k,$$

where $N = 8$ is the number of electrodes of the device.

As illustrated in Extended Data Fig. 2, the average static power consumption $\langle P_{\text{static}} \rangle$ of the measured DNPU is $\sim 1.9 \text{ nW}$. For an estimate of the DNPU power efficiency, we use a conservative value of 5 nW , leading to 320 nW for 64 DNPUs in parallel, which is $\sim 3\times$ lower than realized with analogue filter banks reported in Ref. [33].

TI-46-Word spoken digit dataset

The audio fragments of spoken digits are obtained from the TI-46-Word dataset, available at <https://catalog ldc.upenn.edu/LDC93S9>. To reduce the measurement time, we use the female subset, which contains a total of 2,075 clean utterances from 8 female speakers, covering the digits 0 to 9. The audio samples have been amplified to an amplitude range of -0.75 V to 0.75 V to match the DNPU input range, and trimmed to minimize the silent parts by removing data points smaller than 50 mV (again for reducing measurement time). We used stratified randomized split to divide the dataset into train (90%) and test (10%) subsets.

Software-based feedforward-neural-network training and inference

To evaluate the DNPU performance in reducing the classification complexity, we combined the DNPU preprocessing with two shallow ANNs: (1) a 1-layer feedforward, and (2) a 1-layer convolutional neural network. We trained these two models with both the original dataset and the 32-channel DNPU-preprocessed data. For all evaluations, we used the AdamW⁶¹ optimizer with a learning rate of 10^{-3} and a weight decay of 10^{-5} and trained the network for 200 epochs.

- **Linear layer with the original dataset.** Each digit (0 to 9) in the dataset consists of an audio signal of 1 second length sampled with a 12.5 kS/s rate. Thus, 12,500 samples have to be mapped into one of ten classes. The linear layer, therefore, has $12,500 \times 10 = 125,000$ learnable parameters followed by 10 log-sigmoid functions.
- **Linear layer with the DNPU preprocessed data.** A 10-channel DNPU preprocessing layer with a down-sampling rate of $10\times$ converts an audio signal with a shape of $12,500 \times 1$ into $1,250 \times 10$. Then, the linear layer with $1,250 \times 10 \times 10 = 125,000$ learnable parameters is trained. This model gives $\sim 57\%$ accuracy, which is 2% point less than the 32-channel result reported in Fig. 3.
- **CNN with the original dataset.** The CNN model contains a 1-D convolution layer with one input channel and 32 output channels, kernel size of 8, with a stride of 1, followed by a

linear layer and log-sigmoid activation functions mapping the output of the convolution layer into ten classes. The 1-layer CNN with 32 input and output channels has ~ 4.5 k learnable parameters.

- **CNNs with the DNPU-processed data.** The CNN models used with DNPU preprocessed data contain one (or two) convolution layers with 16/32/64 input channels and 32 output channels followed by a linear layer. Similar to the previous model, we used a kernel size of 8 with a stride of 1 for each convolution kernel. The 1-layer CNN with 16, 32, and 64 channels has ~ 4.5 k, ~ 8.6 k, and ~ 16.9 k learnable parameters, respectively.

AIMC CNN model development

We implemented two CNN models on the AIMC chip with 2- and 3-layer convolutional layers, trained with 32 and 64 channels of DNPU measurement data, respectively. Extended Data Fig. 3 illustrates the architecture of the 3-layer convolution layer with 64 DNPU channels (~ 65 k learnable parameters). The first AIMC convolution layer receives the data from the DNPU with a dimension of 64×1250 . To implement this layer with a kernel size of 8, $64 \times 8 = 512$ crossbar rows are required. To optimize crossbar array resource utilization, this layer has 96 output channels. Thus, in total, 512 rows and 96 columns of the AIMC chip are utilized (Fig. 4c) to implement this layer. The second and third convolution layers both have a kernel size of 3. Considering the 96 output channels, each layer requires $96 \times 3 = 288$ crossbar rows (Fig. 4c). Finally, the fully connected layer is a 36×10 feedforward layer.

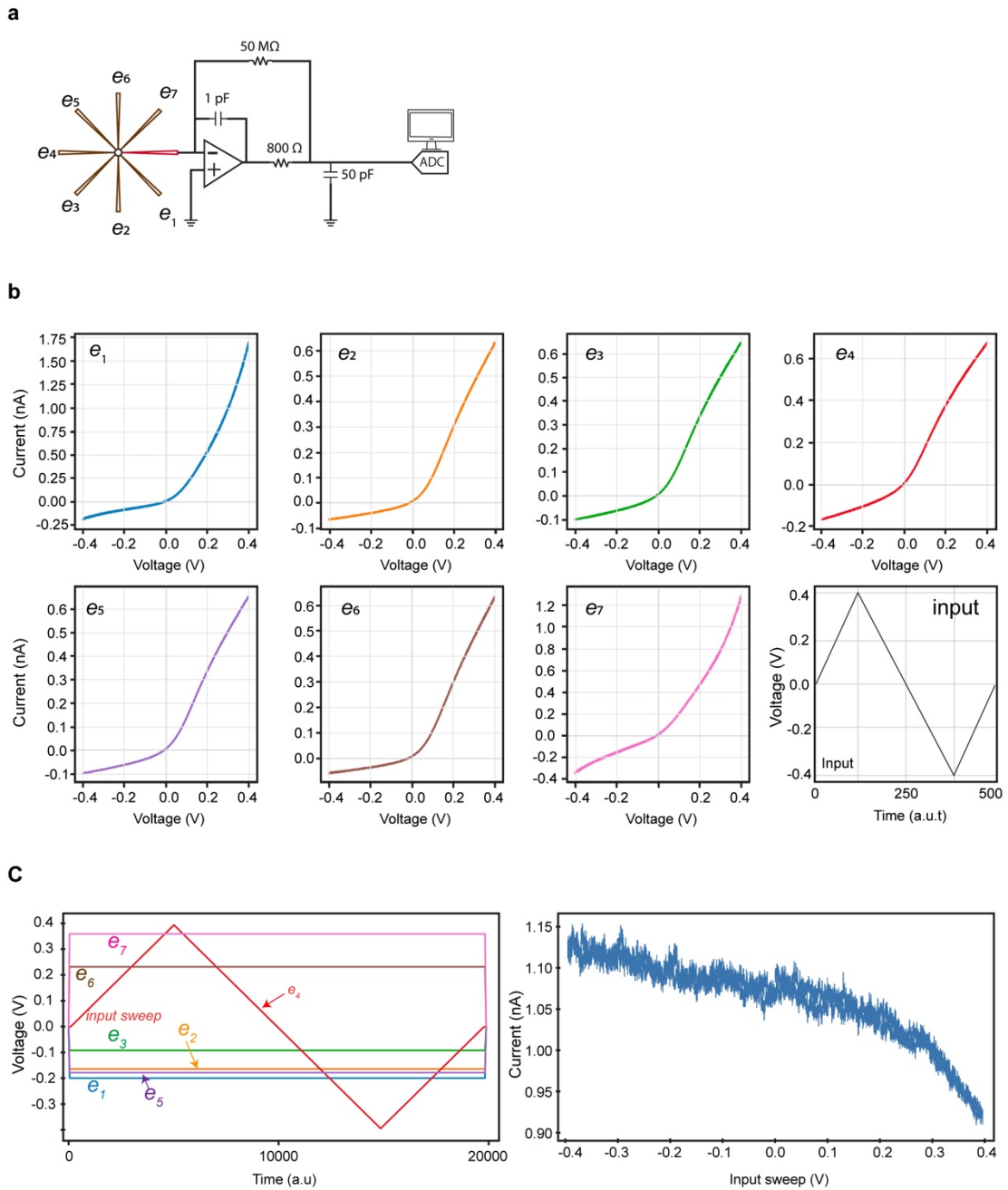
AIMC training & inference

The AIMC training, done in software, consists of two phases: a full-precision phase and a re-training phase, each performed for 200 epochs. The re-training phase is performed to make the classifier robust to weight noise arising from the non-ideality of the PCM devices and the 8-bit input-quantization. During this second phase, we implement two steps: (1) in every forward pass, random Gaussian noise with a magnitude equalling 12% of the maximum weight is added to each layer of the network, as well as Gaussian noise with standard deviation 0.1 is added to the output of every matrix vector

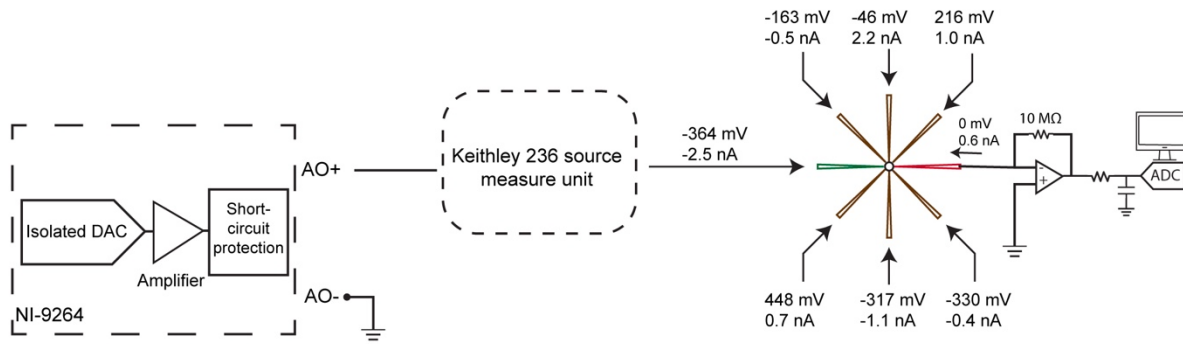
multiplication (MVM) in order to make the model more robust to noise, and (2) after each training batch, weights and biases are clipped to $1.5 \times \sigma_W$ implementing the low-bit quantization, where σ_W is the standard deviation of the distribution of weights.

60 Poindexter, E. et al. Electronic traps and P b centers at the Si/SiO₂ interface: Band-gap energy distribution. *J. Appl. Phys.* **56**, 2844-2849 (1984).

61 Loshchilov, I. & Hutter, F. Decoupled weight decay regularization. Preprint at: <https://arxiv.org/abs/1711.05101> (2017).



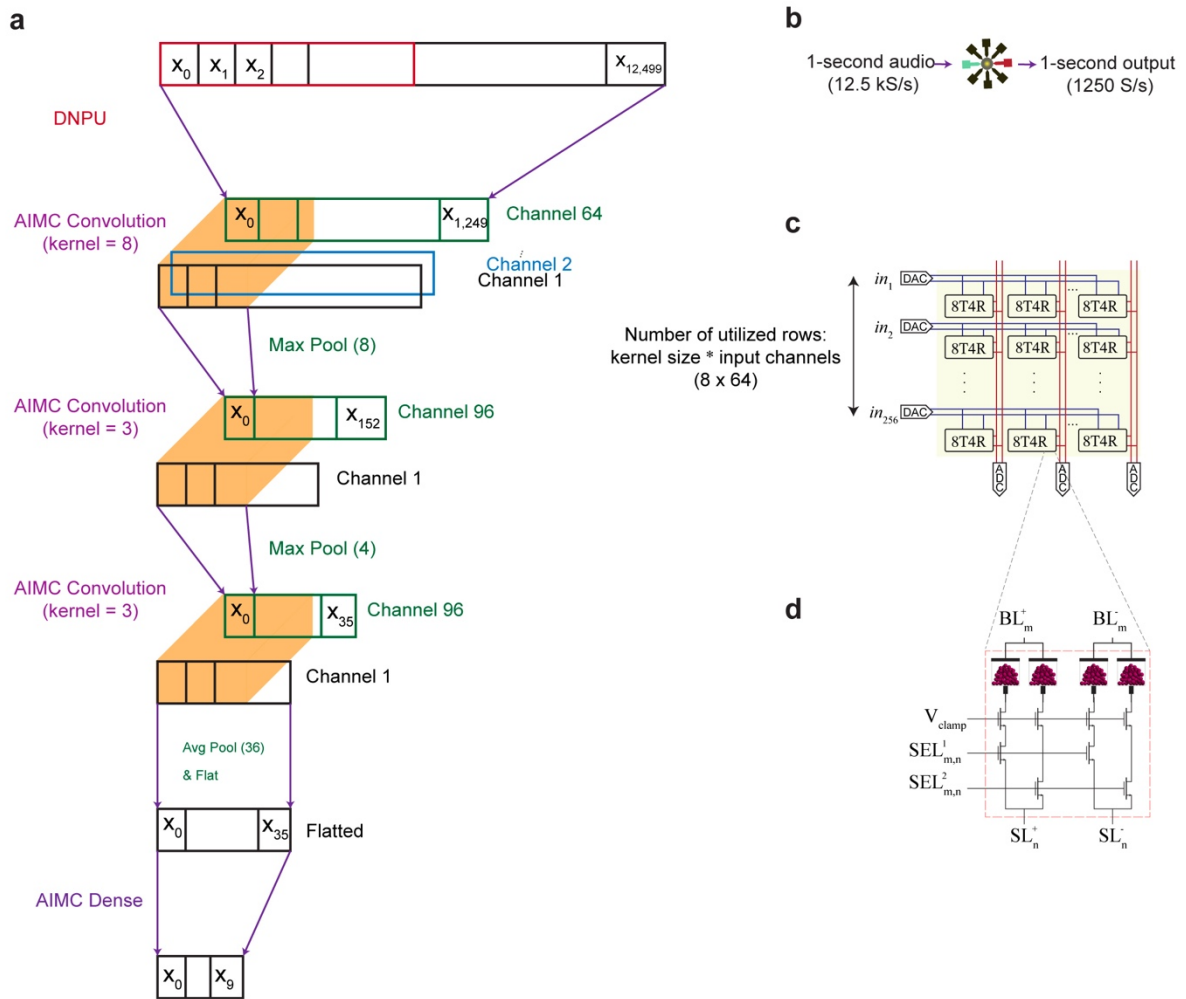
Extended Data Fig. 1. Voltage-in current-out (static) characterization of a boron-doped DNPU. a, Transimpedance (voltage-to-current) amplifier circuit to characterize the device. **b,** Output current of each electrode (e_i) in response to a voltage sweep input from -400 mV to 400 mV, while other electrodes are at zero volt. **c,** (left panel) The input electrode (e_4) receives an input sweep with 400 mV magnitude (shown in red) while the rest of the electrodes are at a constant voltage after an upward ramp from 0 V. (right panel) Output current of the DNPU demonstrating negative differential resistance (NDR).



$$\langle P_{\text{static}} \rangle = \sum V_i I_i$$

$$= 1.9 \pm 0.5 \text{ nW}$$

Extended Data Fig. 2. Schematic of power measurement circuit and an example of measured data. A digital-to-analogue converter (DAC), source measure unit (SMU), and the DNPU are connected in series. For each electrode, the specified voltage is applied by the DAC, and the current is measured with a source measure unit. The measurement is repeated sequentially for each electrode.



Extended Data Fig. 3. Hybrid neural network architecture realized with dopant network processing unit (DNPU) and the IBM HERMES project analogue in-memory computing chip (AIMC). **a**, Network structure. The input to the network is a 1-second audio signal sampled at 12.5 kS/s. The DNPU preprocessing produces 64 vectors of data each with 1,250 samples. Three convolution layers with kernel sizes of 8, 3 and 3 followed by a fully connected layer map the DNPU-processed signal into 10 classes. **b**, The DNPU output is downsampled by a factor of 10 by setting the ADC sampling rate to average every 10 points (oversampling). **c**, The AIMC chip consists of 256 by 256 unit cells. To implement a convolution layer, the crossbar must have a size that includes the kernel size (8 in this example) multiplied by the number of channels (64) in rows. **d**, Each synaptic unit cell of the AIMC chip comprises 4 phase-change-memory devices and 8 transistors (8T4R) organized in a differential configuration to allow for negative weights.

Data availability

Data are available from the corresponding author upon reasonable request.

Code availability

The simulation code and data measured from the DNPU are publicly available on <https://github.com/Mamrez/speech-recognition>.

Acknowledgments

We thank M. H. Siekman and J. G. M. Sanderink for technical support, T. Chen, P. A. Bobbert, U. Alegre-Ibarra, and R. J. C. Cool for stimulating discussions. We acknowledge financial support from Toyota Motor Europe, the Dutch Research Council (NWO) HTSM Grant No. 16237, from the HYBRAIN project funded by the European Union's Horizon Europe research and innovation programme under Grant Agreement No 101046878. This work was further funded by the Deutsche Forschungsgemeinschaft (DFG, German Research Foundation) through project 433682494—SFB1459. This work was also supported by the IBM research AI Hardware Center.

Author contributions

M.Z. and W.G.v.d.W. designed the experiments. L.C. fabricated the DNPU devices. M.Z. and J.B. performed the measurements and simulations. J.B. ported the trained CNN models on the IBM HERMES project chip. All authors discussed the data. M.Z. and W.G.v.d.W. wrote the manuscript and all the authors contributed to revisions. W.G.v.d.W., A.S., and G.S.S. conceived the project. W.G.v.d.W. supervised the project.

Competing interests

The authors declare no competing interests.

Supplementary information is available for this paper at <https://doi.org/xxx>

Correspondence and requests for materials should be addressed to W.G.v.d.W.

Peer review information

Reprints and permissions information is available at <http://www.nature.com/reprints>.

Supplementary Information for

In-materia speech recognition

Mohamadreza Zolfagharinejad¹, Julian Büchel², Lorenzo Cassola¹, Sachin Kinge³,

Ghazi Sarwat Syed², Abu Sebastian², Wilfred G. van der Wiel^{1,4†}

¹NanoElectronics Group, MESA+ Institute for Nanotechnology and BRAINS Center for Brain-Inspired Nano Systems, University of Twente, PO Box 217, Enschede 7500 AE, The Netherlands.

²IBM Research - Europe, Säumerstrasse 4, 8803 Rüschlikon, Switzerland

³Materials Research and Development, Toyota Motor Europe, B-1930 Zaventem, Belgium

⁴Institute of Physics, University of Münster, 48149 Münster, Germany

†Correspondence to: W.G.vanderWiel@utwente.nl

TABLE OF CONTENTS

SUPPLEMENTARY NOTE 1	Recurrent fading memory in DNPU circuit
SUPPLEMENTARY NOTE 2	MAC operations in CNNs for raw audio signal classification
SUPPLEMENTARY NOTE 3	End-to-end training of the DNPU and neural networks
SUPPLEMENTARY NOTE 4	Dataset visualization using uniform manifold approximation and projection (UMAP)
SUPPLEMENTARY NOTE 5	Comparison with low- and band-pass filter banks
SUPPLEMENTARY NOTE 6	Comparison with nonlinear low-pass filter banks
SUPPLEMENTARY NOTE 7	Comparison with nonlinear band-pass filter banks
SUPPLEMENTARY NOTE 8	Comparison with reservoir computing
SUPPLEMENTARY ALGORITHM I	Pseudocode to add harmonics/subharmonics to the filtered signal
SUPPLEMENTARY TABLE I	Inference accuracy comparison among preprocessing methods

1. Recurrent fading memory in DNPU circuit

In a DNPU, the potential landscape of the active region, which is dependent on the potential of the surrounding electrodes, determines the output voltage. In the static measurement mode¹, the output electrode is virtually grounded. In the dynamic measurement mode (this work), however, the output electrode has a finite potential that we read with the ADC. This potential is the charge stored on the capacitor divided by the capacitance ($V_{\text{out}} = Q/C_{\text{ext}}$). The charge on the capacitor, and hence V_{out} , depends on the previous inputs. The short-term (fading) memory of the circuit is therefore *recurrent* in nature, *i.e.*, previous inputs influence the current *physical characteristics* of the circuit over a typical timescale given by the time constant. More specifically, as shown in Fig. 3 of the manuscript, a DNPU circuit is a *stateful* system, where the current behaviour is influenced by past events within a range of tens of milliseconds.

Here, we present some simple experiments to demonstrate this form of recurrent fading memory. For both experiments, we used the DNPU circuit shown in Fig. 1 and Fig. 2 of the manuscript and used the same data acquisition systems as reported in the Methods section with a sampling rate of 25 kS/s.

Supplementary Fig. 1a shows an input pulse series with a magnitude of 1 V (orange) and the output measured from the DNPU (blue). Panels b and c zoom in on the DNPU response. For each panel, we fit an exponential to extract the time constant. The time constant changes over time for the same repetitive input stimulus. We explain this by the output capacitor holding some charge from previous input pulses when the next input pulse arrives. On its turn, the potential landscape of the device is affected by the stored charge, resulting in different intrinsic DNPU impedance values.

Supplementary Fig. 2 emphasizes the *nonlinearity* of the DNPU response, which affects the (dis)charging rate of the DNPU circuit. A series of step functions are fed to the device (orange), and the output is measured and normalized to 1V for better visualization (blue). Each step function has a 200 mV larger magnitude compared to the previous one. The charge stored on the capacitance, read as ADC voltage, is different for each step function, indicating that the DNPU responds to the input nonlinearly, and thus, the time constant for each input step is different. In summary, these two experiments show that the DNPU behaviour is nonlinear, dependent on both the input at $t = t_0$ and on preceding inputs.

2. MAC operations in CNNs for raw audio signal classification

We have implemented the 5-layer convolutional neural network defined in Ref. [62] in PyTorch and calculated the number of MAC operations necessary to execute the inference phase for one input sample. In this model, the first convolution layer requires a receptive field in the order of ~ 10 ms for acoustic feature extraction out of raw audio signals, which, for an input signal sampled with 12.5 kS/s, is equivalent to 125. We used the PyTorch layer-wise OpCounter package (<https://github.com/hahnyuan/pytorch-layerwise-OpCounter>) to profile the number of MAC operations and learnable parameters of each layer. In the defined model, the total number of MAC operations for inference of one input sample with 1 s length is ~ 2.89 M, while the first convolution layer alone requires ~ 2.18 M MACs ($\sim 75.4\%$).

3. End-to-end training of the DNPU and classifier neural networks

DNPU have shown to be reconfigurable for different tasks. Thus, one can envision an end-to-end training framework, where both the classifier and the DNPU are trained together. In Ref. [63], an approach to extract partial derivatives using homodyne gradient extraction (HGE) was proposed for DNPU optimization without the need for a differentiable model. This makes *in-situ* backpropagation possible. Thus, a common optimization algorithm, *e.g.*, gradient descent, can be employed to obtain targeted functionality. Here, we demonstrate a proof-of-concept of the end-to-end training of a 4-channel DNPU feature extractor and a linear layer classifier with backpropagation. A detailed investigation is being prepared for later publication. Supplementary Fig. 3 shows an overview of this approach. For this experiment we used 500 spoken digit samples of female speakers from the TI-46-Word dataset divided into 90% training and 10% test data.

In the forward pass, the audio signal is fed to the DNPU, and the output is measured and stored. The output data have been downsampled by a factor of 10. The linear layer maps these data into 10 classes using the log-sigmoid activation function. In the backward pass, the derivative of the loss function, L , (Cross Entropy Loss) with respect to the linear layer weights, W , is automatically calculated in PyTorch. For the used dataset, the derivative matrix $(\frac{\partial L}{\partial W})$ contains 878 partial derivatives (equivalent to the number of data points in each sample after downsampling), while there exists only one physical DNPU. This is because the DNPU output is a temporal data series, while the neural network maps these points into 10 classes statically. Therefore, to perform the backpropagation using the chain rule, we average these partial derivatives. Finally, to update the DNPU control voltages, first, we calculate the derivatives of the DNPU output with respect to each control voltage for the given DNPU configuration. Then, using the chain rule $(\frac{\partial L}{\partial W} = X^T \frac{\partial L}{\partial Y})$, where X^T is the transposed matrix of the derivatives of the linear layer, and Y the output), we get the gradients of the loss function with respect to the control voltages. Having the derivatives of the loss function with respect to DNPU and linear layer, the optimizer step updates the learnable parameters. The end-to-end training of a 4-channel DNPU with a linear layer gives, on average, ~55% classification accuracy compared to ~40% when the channel DNPU is left untrained (and only the linear layer is trained).

4. Dataset visualization using uniform manifold approximation and projection (UMAP)

Uniform manifold approximation and projection (UMAP)⁵¹ is a nonlinear technique for dimensionality reduction that maps high-dimensional data into low-dimensional data while preserving the local structure in data. Where t-SNE uses a Gaussian kernel to measure the similarity of the points in a high-dimensional space³, UMAP uses a differentiable kernel, which is a weighted combination of two probability distributions. Supplementary Fig. 4 shows the UMAP visualization of the same data visualized with t-SNE in Fig. 3 of the manuscript.

5. Comparison with low- and band-pass filterbanks

The DNPU circuit of Fig. 2a in the manuscript would behave like an ordinary lowpass filter if the DNPU is assumed to be an adjustable *linear* resistor. If so, DNPUs with different control voltages could be used to realize filters with different cut-off frequencies, thus forming a lowpass filter bank. However, as argued above, the DNPU cannot be considered merely a simple linear resistive element.

Figure 2b of the manuscript shows the time constant of the voltage output of the circuit when the input stimulus is a voltage step of 1 volt. When converting the time constants into frequency assuming a linear response, the cut-off frequency of corresponding lowpass filters can be calculated as $f_{cut-off} = \frac{1}{2\pi RC}$, where R and C are the values of the device resistance and the capacitance, respectively. Given the range of the time constants in Fig. 2b, the highest and lowest cut-off frequency of such filters are

$$f_{cut-off,high} = \frac{1}{2\pi RC} = \frac{1}{2\pi \times 12 \times 10^{-3}} = 13 \text{ Hz}, \quad f_{cut-off,low} = \frac{1}{2\pi \times 34 \times 10^{-3}} = 4 \text{ Hz},$$

which are below the lowest frequency the human ear can detect (20 Hz). We used this cut-off frequency range to evaluate the classification accuracy when using a linear lowpass filterbank as feature extractor (Supplementary Table I). However, the simulation results give ~75% classification accuracy. This indicates that the DNPU circuit does not simply construct a linear lowpass filter with the control voltages only changing the cut-off frequency, but rather a nonlinear filter bank that mimics biological cochlea by generating distortion products.

6. Comparison with *nonlinear* low-pass filter banks

To study the effects of nonlinear filtering on the feature extraction step, and consecutively, on the classifier performance, we have introduced *biologically inspired* distortion products to the output of a linear filter, more specifically, distortion products of progressively higher frequency and lower magnitude^{4,5}. Interestingly, these properties are similar to the nonlinear properties of the DNPU. Note that we only intend to qualitatively describe the effect of distortion products on the classification accuracy here, and not to quantitatively represent the DNPU circuit.

The nonlinear filter banks are constructed by adding nonlinear components to the output of a linear time-invariant (LTI) filter. These nonlinear components include (a) harmonic/subharmonic addition and (b) delayed input. In the frequency domain, we progressively decrease the magnitude of the nonlinear components as their frequency increase (please refer to Suppl. Algorithm I for more details).

- a) Harmonic/subharmonic:** Given the input audio signal of $x_{in}(t)$, first, we calculate the Fourier transform of the output of the LTI filter $F(\text{LPF}(x_{in}(t)))$. Then, for a specific range of frequencies, *e.g.*, from the first to the hundredth frequency bin ($[f_0, f_{100}]$), we add that frequency component to the frequency harmonic at the harmonic/subharmonic position ($2 \times f_0, 3 \times f_0, \dots$) divided by the order of the harmonic ($1/n$ for $n \times f_0$). The pseudo-code of this approach is shown in Suppl. Algorithm I.
- b) Delayed inputs:** The second nonlinear property of this nonlinear filtering is to add the delayed output of each filter (with 30% of the magnitude) to the next filter channel for channel > 1 . Although this nonlinear inter-channel crosstalk does not occur in the DNPU circuit, our experiments have shown that this nonlinearity can help improve the classification accuracy. The time delayed has been chosen to be 10 samples, given the 1,250 S/s sampling rate (which is the rate after downsampling the filtered signal).

To evaluate the capability of linear and nonlinear low-pass filter banks in acoustic feature extraction, we used a similar pipeline for DNPU-processed data, *i.e.*, a 1-layer CNN with a kernel size of 3, a *tanh* activation function trained for 500 epochs with the AdamW⁶¹ optimizer and a learning rate and weight

decay of 0.001. We have also used the OneCycleLR scheduler⁶⁴ with a maximum learning rate of 0.1 and a cosine annealing strategy. The classifier model has been intentionally kept simple to limit its feature extraction capabilities so that we can better evaluate different preprocessing methods.

We examined linear low-pass filter banks under two scenarios: (1) setting the cut-off frequencies according to the DNPU circuit time constants, *i.e.*, 4 and 13 Hz, for lower and higher limits, respectively. And (2) setting a wider range of cut-off frequencies, *i.e.*, 20 and 625 for lower and higher limits, respectively. The higher limit for the latter case is based on the Nyquist frequency given the 1,250 S/s sampling rate. The inference accuracy results for the same TI-46-Word benchmark test are summarized in Suppl. Table I.

7. Comparison with nonlinear band-pass filter banks

The hair cells of the basilar membrane in the cochlea convert acoustic vibrations into electrical signals *nonlinearly*, where small displacements cause a significant change in the output at first. However, as the displacements increase, this rate slows down and eventually approaches a limit. It has been proposed that this *compressive nonlinearity* (CN) can be modelled as a *hyperbolic tangent* (tanh) function⁵. Similar to nonlinear low-pass filter banks (see Suppl. Note 5), we implemented a nonlinear *band-pass* filter bank as a model for auditory filters in the mammalian auditory system. The model is constructed by an LTI filter bank of band-pass filters ($f_{b_{\text{band-pass}}}$) initialized with gammatone within 20 Hz to 625 Hz followed by the tanh nonlinearity described as follows:

$$f_{\text{CN}}(X) = \frac{1}{2} \times \tanh(f_{b_{\text{band-pass}}}(X) + 1),$$

where X represents the input audio signal. For simulations with this nonlinear band-pass filter bank, we use the same classifier model (1-layer CNN) with the same hyperparameters described in Suppl. Note 5. The performance of this nonlinear filter bank is summarized in Suppl. Table I. Remarkably, adding the tanh nonlinearity increases the overall classification accuracy to over 93%, which is significantly higher than the LTI band pass filter bank but still less than the value obtained with DNPU preprocessing.

8. Comparison with reservoir computing

Here we make a comparison with reservoir computing (RC), in particular with echo state networks (ESNs). ESNs are RC-based frameworks for time-series processing, which are essentially randomly initialized recurrent neural networks⁶⁵. ESNs offer *nonlinearity* and *short-term memory* essential for projecting input data into a high-dimensional feature space, where the classification of those features becomes simpler. As reported in the main text, most RC solutions for speech recognition rely on frequency-domain feature extraction. More specifically, a reservoir is normally used to project *pre-extracted* features into a higher dimensional space, and then, a classifier, often a linear layer, is used to perform the classification.

Here, we compare the efficacy of ESNs for acoustic feature extraction to DNPU and filter banks. Using the ReservoirPy Python package⁶⁶, we modelled 64 different reservoirs initialized with random conditions for *neuron leak rate* (*lr*), *spectral radius of recurrent weight matrix* (*sr*), *recurrent weight matrix connectivity* (*rc_connectivity*), and *reservoir activation noise* (*rc_noise*). Then, the same dataset as described in the main text is fed to all these reservoir models, and the output is used for classification. The reservoir maps the input to output with a down sampling rate of 10×, the same as for DNPU and filter banks. We used the same classifier model and hyperparameters described in Suppl. Info. Note 5. The performance of using reservoirs as feature extractors is summarized in Suppl. Table I. Notably, this approach performs the poorest among other feature extractors. We attribute this low classification rate to the absence of bio-plausible mechanisms for acoustic feature extraction in the reservoir system. More specifically, although a reservoir projects the input into a higher-dimensional space, the lack of *compressive linearity*, a *recurrent* form of *feedback* from the output, and *frequency selectivity* make acoustic feature extraction with reservoirs less effective compared to other solutions.

References

- 62 Dai, W., Dai, C., Qu, S., Li, J. & Das, S. Very deep convolutional neural networks for raw waveforms. In *2017 IEEE International Conference on Acoustics, Speech and Signal Processing (ICASSP)* 421-425 (IEEE, 2017).
- 63 Boon, Marcus N. et al. Gradient descent in materio. Preprint at: <https://arxiv.org/abs/2105.11233>
- 64 Smith, Leslie N., Topin, N. Super-convergence: Very fast training of neural networks using large learning rates. Preprint at: <https://arxiv.org/abs/1708.07120>
- 65 Jaeger, H. The “echo state” approach to analysing and training recurrent neural networks-with an erratum note. *Bonn, Germany: German National Research Center for Information Technology GMD Technical Report* **148**, 13 (2001).
- 66 Trouvain, N., Pedrelli, L., Dinh, T. T. & Hinaut, X. *ReservoirPy: An Efficient and User-friendly Library to Design Echo State Networks*. In *2020 International Conference on Artificial Neural Networks and Machine Learning* 494-505 (ICANN, 2020)

```
1  Procedure non-linear-filter(signal, cutoff, h_num, sh_num)

2      lpf_signal  $\leftarrow$  LPF(signal)

3      freq_bins  $\leftarrow$  rfft.freq(signal)

4      fft_lpf_signal  $\leftarrow$  rfft (lpf_signal)

5      for f := 1 to 100 do
6          fft_lpf_signal[f]  $\leftarrow$  0.9  $\times$  fft_lpf_signal[f]
7          for h := 2 to h_num do
8              fft_lpf_signal[where(freq_bins == h  $\times$  freq_bins[f])] +=
9                   $\frac{1}{h} \times$  fft_lpf_signal[f]
9      Endfor

10     for f := 100 to 200 do
11         for sh := 2 to sh_num do
12             fft_lpf_signal[where(freq_bins ==  $\frac{\text{freq\_bins}[f]}{sh}$ )] +=
13                  $\frac{1}{sh} \times$  fft_lpf_signal[f]
13         Endfor
14     return irfft(fft_lpf_signal)
```

SUPPLEMENTARY TABLE I. INFERENCE ACCURACY COMPARISON AMONG PREPROCESSING METHODS

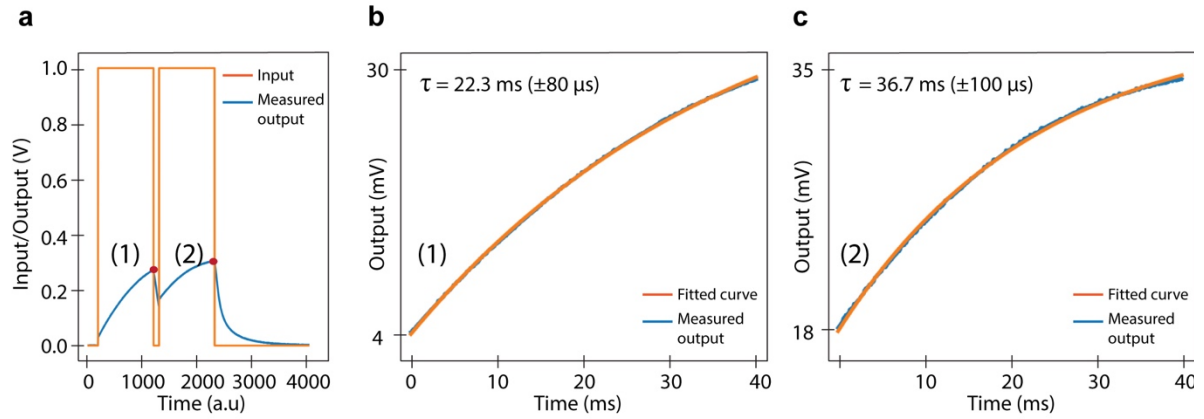
Preprocessing type (64-channels)	Cut-off freq. range (lower, higher) Hz	Accuracy
Reservoir ^a	N.A.	~51%
Low-pass	4 – 13	75.5%
Non-linear low-pass	4 – 13	77.9%
Low-pass	20 – 625	80.3%
Non-linear low-pass	20 – 625	85.1%
Band-pass ^b	20 – 625	85.1%
Gammatone ^c	20 – 625	83.2%
Non-linear gammatone ^d	20 – 625	93.8%
DNPU	N.A.	95.7%

^a Averaged for 10 runs with different reservoir models and noise levels.

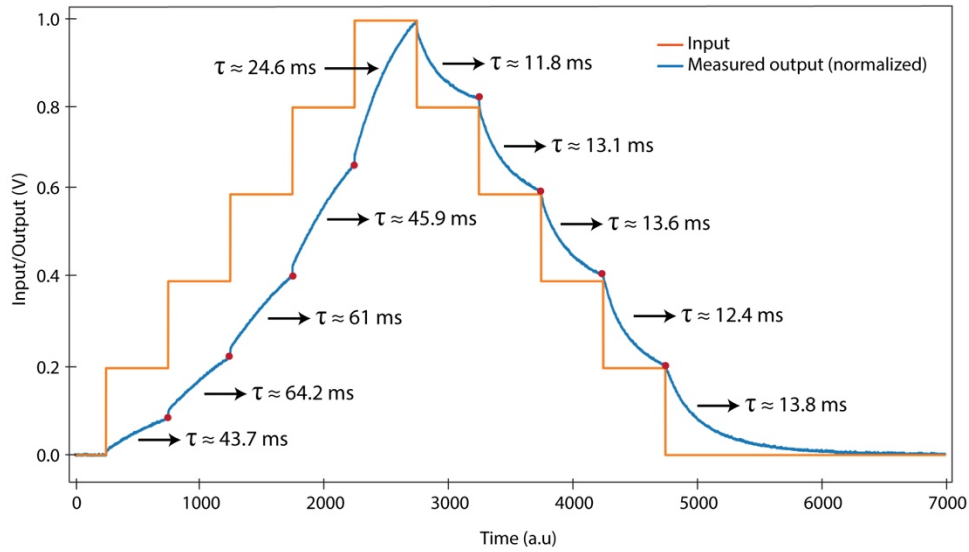
^b Linearly spaced cut-off frequencies, bandwidth = 25 Hz.

^c Linearly spaced cut-off frequencies.

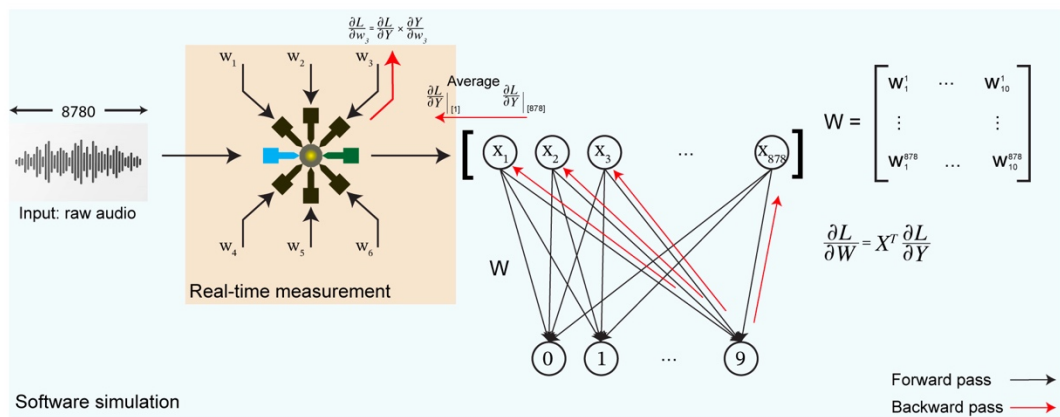
^d Linearly spaced cut-off frequencies, gammatone initialization with *tanh* compressive nonlinearity.



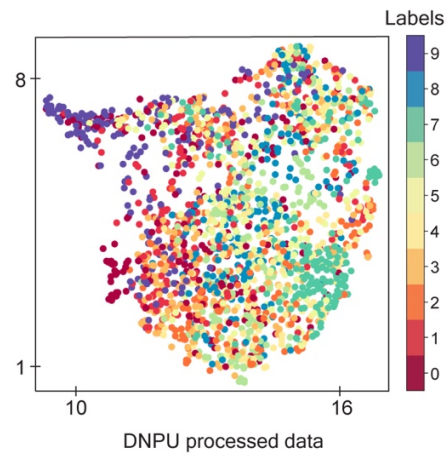
Supplementary Fig. 1. Output response analysis of the DNPU circuit to input pulses. **a**, The DNPU circuit shown in the Fig. 2 and Fig. 3 of the manuscript is fed with input pulses staircase-like input signal (orange) and the output (blue) is measured. The measurement sampling rate is set to 25 kS/s. **b**, The output response to the first input pulse is shown in blue and the fit to the curve in orange. Based on the fitted curve, the time constant τ is calculated to be 22.3 ms. **c**, The output response to the second input pulse is shown in blue and the fit to the curve in orange. The time constant is calculated to be 36.7 ms. The change in the time constant, *i.e.*, the DNPU resistance and its internal capacitance, indicates that the charge stored on the capacitance influences the device behaviour in a recurrent form.



Supplementary Fig. 2. Output response analysis of the DNPU circuit to a staircase input. The DNPU circuit shown in Fig. 2 and Fig. 3 of the manuscript is fed with a staircase-like input signal (orange) and the output (blue) is measured and normalized to one. In contrast to a linear time-invariant (LTI) RC circuit, the resistance of the DNPU is a nonlinear function of the input as well as the charge stored on the external capacitance. The time constant of each step is calculated by fitting an exponential to the output in software.



Supplementary Fig. 3. End-to-end training of a DNPU with a feedforward linear layer neural network for speech recognition. A linear layer neural network is simulated in software while a physical is being measured for iterative training of the network using backpropagation. The gradients of the DNPU are extracted *in situ* during the backward pass using the homodyne gradient extraction (HGE) method. The optimizer simultaneously updates the control voltages and the parameters of the neural network.



Supplementary Fig. 4. Uniform manifold approximation and projection (UMAP) visualization of DNPu preprocessed dataset. The preprocessed data are the same as used for the t-SNE visualization in Fig. 3 in the manuscript.